Check for updates

Germanium-Functionalized 3D Microporous, Nanostructured Nickel-Nickel Oxides for Application in Asymmetric Supercapacitors

Balwant Kr Singh, Debabrata Das, Cristina Gonzalez, and C. V. Ramana*

Supercapacitors and batteries are essential for sustainable energy development. However, the bottleneck is the associated high cost, which limits bulk use of batteries and supercapacitors. In this context, realizing that the cost of energystorage device mainly depends on materials, synthesis processes/procedures, and device fabrication, an effort is made to rationally design and develop novel low-cost electrode materials with enhanced electrochemical performance in asymmetric supercapacitors. Herein, surface functionalization approach is adopted to design low-cost 3D mesoporous and nanostructured nickel-nickel oxide electrode materials using facile synthesis for application in supercapacitors. It is demonstrated that the 3D mesoporous Ni provides the high surface area and enhanced ionic conductivity, while germanium functionalization improves the electrical conductivity and reduces the charge-transfer resistance of NiO. Surface functionalization with Ge demonstrates the significant improvement in specific capacitance of NiO. The asymmetric supercapacitor using these Gefunctionalized NiO-Ni electrodes provides a specific capacitance of 304 Fg⁻¹ (94 mF cm⁻²), energy density of 23.8 Wh kg⁻¹ (7.35 μ Wh cm⁻²), and power density of 6.8 kW kg⁻¹ (2.1 mW cm⁻²) with excellent cyclic stability of 92% after 10 000 cycles. To validate their practical applications, powering the digital watch using the asymmetric supercapacitors in laboratory conditions is demonstrated.

1. Introduction

Climate change, global warming, depletion of fossil fuels, and increasing energy demand coupled with rapidly increasing global population have pushed society toward the use of clean and sustainable energy technology. [1–8] Undoubtedly, the ultimate, unique, and only solution to all these problems is clean and sustainable energy technology, which gives us clean energy from renewable sources like solar, wind, and water. [9,10]

B. Kr Singh, D. Das, C. Gonzalez, C. V. Ramana Centre for Advanced Materials Research (CMR) University of Texas at El Paso 500 W University Avenue, El Paso, TX 79968, USA E-mail: rvchintalapalle@utep.edu

D. Das, C. Gonzalez, C. V. Ramana Department of Aerospace and Mechanical Engineering University of Texas at El Paso 500 W University Avenue, El Paso, TX 79968, USA

The ORCID identification number(s) for the author(s) of this article can be found under https://doi.org/10.1002/ente.202300360.

DOI: 10.1002/ente.202300360

However, natural sources of clean and sustainable energy are not available all the time; therefore, energy-storage and conversion technologies are very essential for their continuous use. Further, to reduce carbon emissions, there is also a rapid increase in electric vehicles, which cannot run without energy-storage units. Apart from this, over time, the progressing use of portable electronic devices and standalone remote internet of things platforms has also increased the need for energy-storage units. [5,11,12]

The energy and/or power applications employ batteries and supercapacitors, where the choice is typically based on the requirements of high-energy and high-power density. Due to its high energy density (\approx 180 Wh kg $^{-1}$), the battery is the first choice of consumer electronics devices. However, low power density, sluggish charge transport, and dendrites formation at high power impede its wider use. In contrast, high power density (\approx 10 W kg $^{-1}$), fast charge–discharge times, and long cyclic life (>100 000) make supercapacitors

more attractive and useful than batteries for peak power applications. [4,13] Depending on materials, the charge-storage mechanism of the supercapacitor is divided into two types, electrical double layer capacitor (EDLC) and pseudocapacitor. All carbon-based materials show EDLC behavior where the charge is stored at the electrode-electrolyte interface. Transition-metal oxides/nitrides and conducting polymer show pseudocapacitive behavior where the charge is stored due to faradaic redox reaction. [14–17] Various inorganic and organic composites with carbon-based nanostructures, such as graphene and carbon nanotube, can improve the overall capacitance drastically through bidirectional enhancement of both charge-storage strategies.[15-17] As a result, supercapacitor offers the potential to fill the gap between high energy-density batteries and traditional high-power density dielectric capacitors. Furthermore, compared to solid-state or lithium/sodium-ion batteries, supercapacitors have several advantageous characteristics, including safe operation, cost-effectiveness, high specific capacitance, quick charge/discharge capacity, and exceptional power density. Therefore, in recent years, supercapacitors attracted a lot of attention from the scientific and engineering community with a special focus on the design and development of new materials

21944296, 2023, 10, Downloaded from https://onlinelibrary.wiley.com/doi/10.1002/ene.202300360 by The University Of Texas El Paso, Wiley Online Library on [10.07/2024]. See the Terms and Conditions (https://onlinelibrary.wiley

.com/terms-and-conditions) on Wiley Online Library for rules of use; OA articles are governed by the applicable Creative Commons License

utilizing nanostructured assemblies and hybrid architectures for enhanced performance.

In the context of novel materials, design, and development. considerable attention has been paid to the transition-metal oxide electrodes to enhance performance in symmetric and symmetric supercapacitors. Among transition-metal oxides, nickel oxide (NiO) is the most studied material for energy applications, in general, and particularly for supercapacitor applications. NiO exhibits unique structural, electrical, optical, and electrochemical characteristics.^[1,18-24] Based on the structure and properties, NiO finds applications in various domains, such as ammonia sensors, [18] electrocatalysts for oxygen evolution processes, [1,19] photo-electrode in dye-sensitized solar cells, [20] cathode materials for quasi-solid-state lithium-ion batteries, [21] and electrochromic supercapacitor.^[22] Nickel oxide- and NiO-based materials offer promising options for electrochemical energy applications owing to their advantageous electrochemical characteristics, good thermal stability, cheaper cost, wider availability, nontoxicity, and environmental stability. The theoretical capacitance of NiO is 3750 Fg⁻¹, which is higher than that of MnO₂ (1370 Fg⁻¹) and hydrated RuO₂.nH₂O (2200 Fg⁻¹).^[22,23] Despite the encouraging properties of NiO, the poor electrical conductivity^[24] and phase change during charge-discharge hindered its bulk or widespread applications.

As documented in the literature, various approaches have been developed to overcome the poor electrical conductivity of NiO. Nickel oxides-carbon composites and bimetal oxides composites and doping in nickel oxides were some of them which resulted in some improvements. [22,25,26] Among these approaches adopted, the surface fictionalization of metal oxides is a simple and efficient approach, which can result in desirable surface and electronic properties. It has been demonstrated that the surface fictionalization in Ni oxides enhances their electrical conductivity, creates an efficient diffusion path, and introduces oxygen vacancies, all of which improve overall supercapacitor performance. [27,28] In this work, we propose and present a simple approach based on the surface functionalization of NiO electrode materials with germanium (Ge) to achieve their enhanced performance in supercapacitors. Being the widely known semiconductor. Ge offers many advantages like high electrical conductivity, high electron mobility, small bandgap (0.6 eV), and enhanced electron transfer by reducing the interfacial recombination. [2,6] In fact, Ge-based anode materials were proved to be the promising candidate materials for next-generation battery applications.^[29,30] Therefore, the entire device structure derived from those materials compatible with consumer and traditional power electronics, the proposed Ge-functionalized NiO materials may overcome the problems associated with electrode materials for supercapacitor applications.

The performance of supercapacitors is principally dependent on the surface area and electrical conductivity of electrode materials. The 3D porous linked metal network offers a high surface-to-volume ratio and open channel for electrolyte diffusion. With similar advantages in mind, interconnected nanoporous gold (Au) was already employed in energy-storage and conversion applications, such as supercapacitors, batteries, and electrocatalysis. [31-33] However, the high cost of Au restricts widespread usage, particularly not suitable for most commercial applications. Therefore, economically viable and cheaper alternatives for the production of porous metals with similar properties are highly desirable. In this context, we propose Ni- and NiO-based materials' design and development with a surface functionalization approach to meet the economic and performance requirements of supercapacitors. In most cases, Ni is purchased in the form of films, foils, and foams to use in energy-related applications, which leads an increase to the overall device cost. Germanium incorporation in the metal oxide matrix improves its electrical conductivity and reduces charge transfer resistance.[34] Considering the aforementioned challenges and advantages, here in the present work, we demonstrate a systematic procedure to achieve 3D mesoporous Ge/NiO nanostructure as an active electrode material on affordable, cheap, and electronically well-adopted Cu substrates. We employed an electrodeposition technique to deposit these 3D mesoporous Ni onto the Cu substrate. To improve the electrical conductivity of metal oxide, Ge was conformally deposited onto 3D porous Ni by using sputter deposition, which is a widely adopted industrial method to deposit thin films on surfaces and interfaces in microelectronic circuits. In our approach, thermal treatment at moderate temperature (400 °C) was performed after the Ge-surface functionalization to make the samples homogeneous. The approach adopted in this work is schematically presented in Figure 1. The conformal deposition of Ge onto a 3D mesoporous Ni skeleton and thermal oxidation creates the Ge-functionalized NiO (GeNiO), which lowers the overall interface contact resistance by enabling enhanced electron transport across an interconnected porous Ni network and easier ion accessibility through mesoporous channels. As presented and discussed in this paper, the 3D mesoporous GeNiO nanostructures exhibit excellent electrochemical performance when used as a positive electrode for asymmetric supercapacitor configuration.

2. Results and Discussion

2.1. Crystal Structure, Morphology, and Composition

The X-Ray diffraction (XRD) data of Ge-NiO samples are shown in Figure 2, where the visible diffraction peaks are located at 44.33°, 44.47°, 51.4°, 51.81°, 74.9°, and 77.33°. The peaks at



Figure 1. Schematic representation of the surface-functionalization approach employed for NiO electrodes. The sequence of steps represents starting from bare Cu substrates onto which the 3D mesoporous Ni was electrodeposited, followed by Ge functionalization of the surface. The final material is a 3D mesoporous Ge-NiO nanostructure onto Cu substrate.

21944296, 2023, 10, Downloaded from https:/

//onlinelibrary.wiley.com/doi/10.1002/ente.202300360 by The University Of Texas El Paso, Wiley Online Library on [10.07/2024]. See the Terms and Conditions (https://onlinelibrary.wiley

and-conditions) on Wiley Online Library for rules of use; OA articles are governed by the applicable Creative Commons Licenso

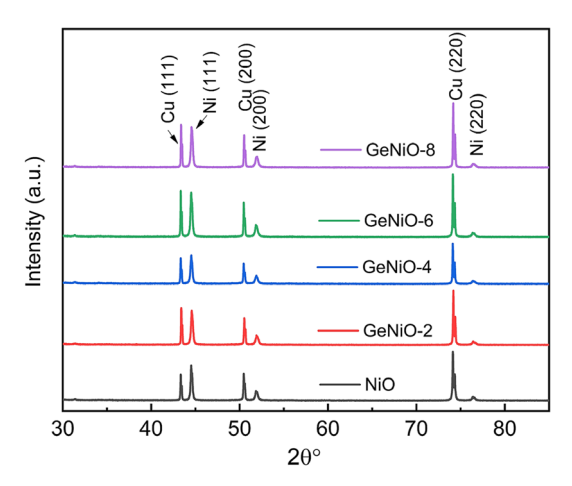


Figure 2. X-ray diffraction (XRD) patterns of 3D mesoporous nickel-germanium-nickel oxides on the copper substrate after annealing 400 °C for 30 min. The data shown are for samples prepared under variable deposition time of Ge.

44.33°, 51.4°, and 74.9° correspond to diffraction from (111), (200), and (220) planes of metallic Cu (matches to ICDD number 00-003-1018). The peaks at 44.47°, 51.81°, and 77.33° correspond to the (111), (200), and (220) planes of metallic Ni (matches with ICDD 00-03-1015). The XRD peaks of Cu and Ni observed are in good agreement with the literature.[35,36]

The scanning electron microscope (SEM)-determined surface morphology of the Ge-NiO samples is shown in Figure 3. The data shown in Figure 3a,b is the surface morphology features of 3D-microporous Ni before and after annealing at 400 °C. It is

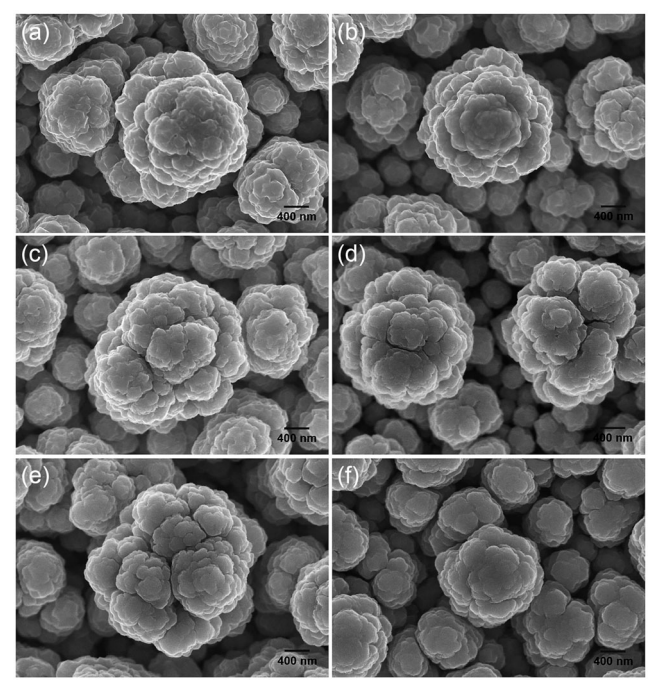


Figure 3. Scanning electron microscope (SEM) images of electrodeposited NiO on 3D microporous Ni and after annealing 400 °C for 30 min. The data shown are for a) 3D microporous Ni, b) NiO, c) GeNiO-2, d) GeNiO-4, e) GeNiO-6, and f) GeNiO-8.

evident that the 3D-microporous Ni exhibits cauliflower floretstype morphology, which is routinely seen in electrodeposited Ni under optimum conditions. Figure 3c-f depicts the surface structure of Ge coated for 2, 4, 6, and 8 min on 3D-microporous Ni after annealing at 400 °C, respectively. With the increasing deposition time of Ge, the surface edge of 3D microporous fades, as shown in Figure 3c-f. The Ge-functionalized 3D microporous Ni/NiO structure with high surface area and open pores is essential for supercapacitor applications.

Figure 4 shows the elemental mapping of nickel (Ni), oxygen (O), and germanium (Ge) in the Ge-NiO with Ge-deposition time varied from 0 to 10 min. Energy dispersive X-ray spectroscopy (EDS) data indicates that the concentration of Ge increases with increasing deposition time. It can also be observed that the deposited Ge on the surface resides mostly on the top of the Ni cauliflower florets structures.

Finally, the NiO nanoflakes sample was deposited to Ge-NiO-4 to further improve supercapacitor performance. Figure 5a shows the XRD data of NiO nanoflakes after electrodeposition. Only metallic peaks of Ni and Cu are present. The absence of NiO peaks may be due to its amorphous nature or small quantity compared to Ni or Cu. Figure 5b depicts the surface morphology of NiO nanoflakes. The conformal deposition of NiO nanoflakes nanostructure on Ge-functionalized 3D mesoporous Ni improves the electrode surface area, which further enhances the capacitance. The elemental mapping (Figure 5c,d) reveals that the homogeneous distribution of different elements present on the material's surface. The results convincingly show the presence of Ni, O, and Ge, while Ge concentration is more at the top surface around the cauliflower grains. As demonstrated later in electrochemical characterization, the presence of Ge on the surface helps to improve the electrical conductivity of NiO.

2.2. Electrochemical Characterization and Performance Characteristics

As a first step toward evaluating the electrochemical performance of the electrode materials developed in this work, we performed the cyclic voltammetry measurements, which also helped us understand the charge-storage mechanism and performance of Ge-functionalized Ni/NiO. The electrochemical measurements were performed in a 3-electrode system, where platinum and Hg/HgO were used as counter and reference electrodes, respectively. The electrochemical measurements were done in 3 M KOH at 2–200 mV s⁻¹ scan rates. **Figure 6**a–e shows the voltammogram of NiO, GeNiO-2, GeNiO-4, GeNiO-6, and GeNiO-8 at different scan rates. It is evident that the peak current density increases with increasing scan rate in all the samples. Figure 6f compares bare and Ge-functionalized NiO at different scan rates. The maximum specific capacitance of $53\,\mathrm{mF\,cm}^{-2}$ is achieved in the case of GeNiO-4 at a scan rate of 2 mV s⁻¹. The pair of anodic and cathodic peaks between 0.3 and 0.6 V shows the faradaic nature of NiO. The peaks indicate pseudocapacitive behavior, where Ni changes its state from Ni²⁺ to Ni³⁺, similar to what was previously reported in the literature. [37,38] The pair of redox reactions during oxidation and reduction of nickel oxides can be explained by the following equation^[39,40]

21944296, 2023, 10, Downloaded from https

onlinelibrary.wiley.com/doi/10.1002/ente.202300360 by The University Of Texas El Paso, Wiley Online Library on [10/07/2024]. See the Terms

onditions) on Wiley Online Library for rules of use; OA articles are governed by the applicable Creative Commons License

Figure 4. EDS elemental mapping of 3D mesoporous Ni-NiO-Ge with different deposition times of germanium and after annealing 400 °C for 30 min. The data shown are a-e) GeNiO-2, f-j) GeNiO-4, k-o) GeNiO-6, and p-t) GeNiO-8.

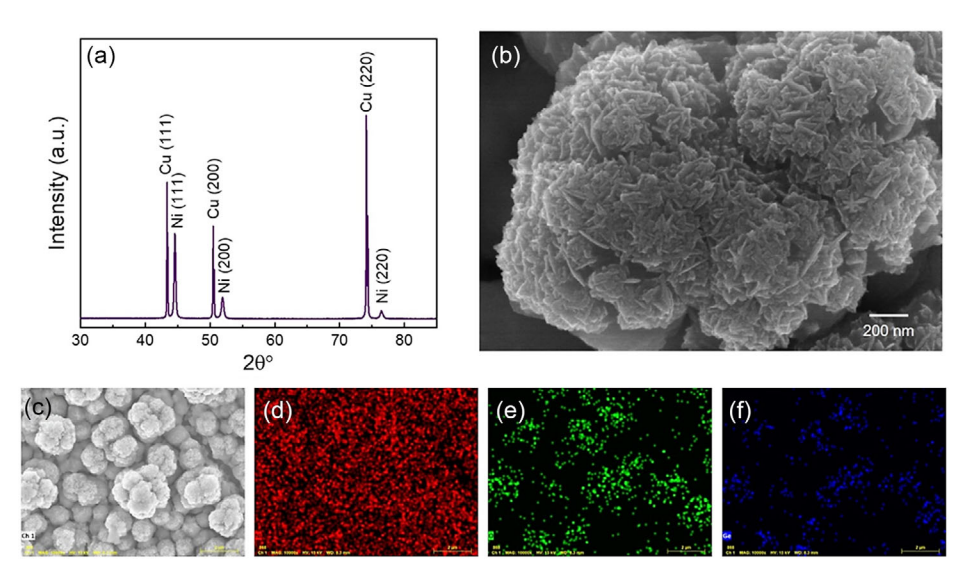


Figure 5. The material characterization data of Ge-functionalized NiO nanoflakes on 3D mesoporous Ni. The data shown here are a) XRD, b) SEM image of NiO, and c-f) EDS elemental mapping indicating the distribution of Ni, O, and Ge.

$$NiO + OH^- \leftrightarrow NiOOH + e^-$$
 (1)

The galvanic charge-discharge characteristics of Gefunctionalized NiO at different current densities in a potential window of 0.2-0.6 V are shown in Figure 7a-e. It can be seen that, in all the samples, charge-discharge time increases with decreasing current density. The nonlinear behavior of the charge-discharge curve indicates the pseudocapacitive nature of NiO, [41] which also agrees with cyclic voltammetry data, as shown in Figure 6. The specific capacitance variation at different current density is depicted in Figure 7f. The higher charge-discharge time is obtained in Ge-NiO-4. The maximum capacitance is obtained in the case of 43 mF cm⁻² at the current density of $1.75 \,\mathrm{mA \, cm^{-2}}$.

The electrochemical characterization data of NiO nanoflakes deposited on GeNiO-4 are shown in Figure 8. The cyclic voltammogram at different scan rates is shown in Figure 8a, where the presence of a pair of oxidation and reduction indicates the pseudocapacitive nature of NiO nanoflakes. The peak current increases with an increasing scan rate. The specific capacitance at different scan rates determined from cyclic voltammetry is shown in Figure 8b. The maximum specific capacitance achieved is $768 \,\mathrm{mF} \,\mathrm{cm}^{-2}$ (2135 Fg $^{-1}$) at a scan rate of $2 \,\mathrm{mV} \,\mathrm{s}^{-1}$. The specific capacitance increases at lower scan rates. This is due to the fact that at lower scan rates, electrolyte ion has more time to reach into the bulk of materials, while at higher scan rates, electrolyte ion movement is limited to near-surface region.[33,42] Figure 8c shows the charge-discharge of NiO nanoflakes at different

21944296, 2023, 10, Downloaded from https:

//onlinelibrary.wiley.com/doi/10.1002/ente.202300360 by The University Of Texas El Paso, Wiley Online Library on [10/07/2024]. See the Terms

and Condit

and-conditions) on Wiley Online Library for rules of use; OA articles are governed by the applicable Creative Commons License

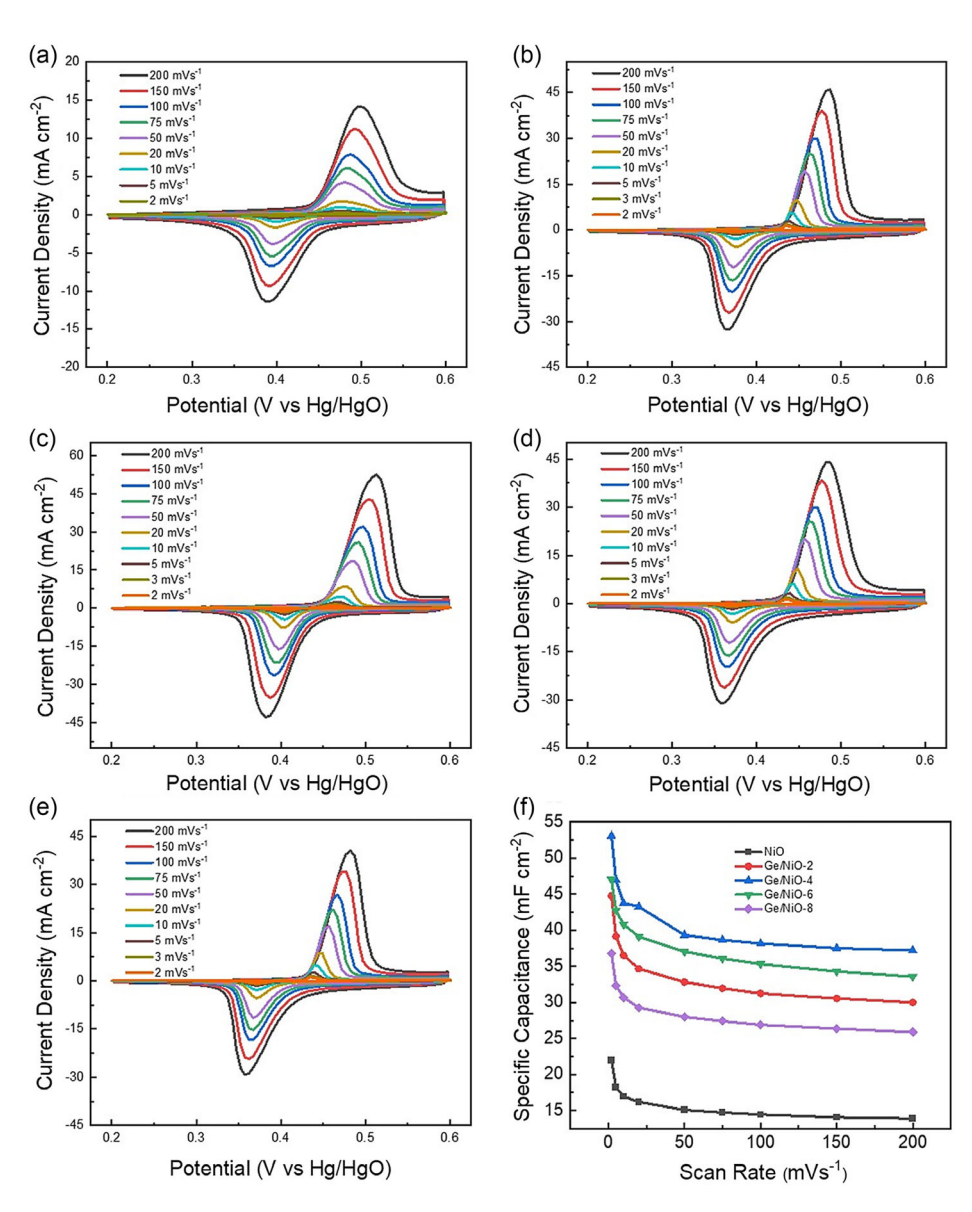


Figure 6. Cyclic voltammetry of Ge functionalized 3D mesoporous Ni/NiO with different deposition times of Ge and after annealing 400 °C for 30 min. The data shown are a) NiO, b) GeNiO-2, c) GeNiO-4, d) GeNiO-6, e) GeNiO-8, and f) comparison of specific capacitance variation with respect to different scan rates.

current values. The nonlinear charge-discharge curve shows the pseudocapacitive nature of NiO nanoflakes. The maximum specific capacitance we obtained was 457 mF cm⁻² (1269 Fg⁻¹) at a current density of 4.3 mA cm⁻². The relation between peak currents and scan rates is depicted in Figure 8d. The linear relation between peak currents and the square root of scan rates suggests that the charge-storage mechanism is dominated by a semi-infinite bulk diffusion process. The charge-storage mechanism of a pseudocapacitive material can be deduced from the cyclic voltammetry experiment by plotting peak currents as a function of scan rates. While the peak current for a surface redox reaction varies directly with scan rates, the peak current for a semi-infinite bulk diffusion process changes with the square root of scan rates.^[43,44] To understand the capacitance retention of NiO nanoflakes, cyclic stability measurements were made for

10 000 cycles at a current density of 34.5 mA cm⁻². It holds 92% capacitance retention after 5000 cycles and decreases \approx 80% after 10 000 cycles, as shown in Figure 8f. Compared to the literature, the obtained results in this work are far better in some cases and comparable with others. The detailed comparison is presented in Table S1, Supporting Information.

Finally, the performance and stability were evaluated for asymmetric configuration fabricated using Ge-functionalized NiO nanostructures as the positive electrode and activated carbon as the negative electrode. For the asymmetric configuration, activated carbon was optimized on a nickel sheet (Figure S1, Supporting Information). Figure 9a shows the schematic of the asymmetric supercapacitor connected to a battery. The cyclic voltammetry response (Figure 9b) of both Ge-functionalized NiO nanostructured and activated carbon were measured in

21944296, 2023, 10, Downloaded from https:

//onlinelibrary.wiley.com/doi/10.1002/ente.202300360 by The University Of Texas EI Paso, Wiley Online Library on [10/07/2024]. See the Terms and Condit

s-and-conditions) on Wiley Online Library for rules of use; OA articles are governed by the applicable Creative Commons License

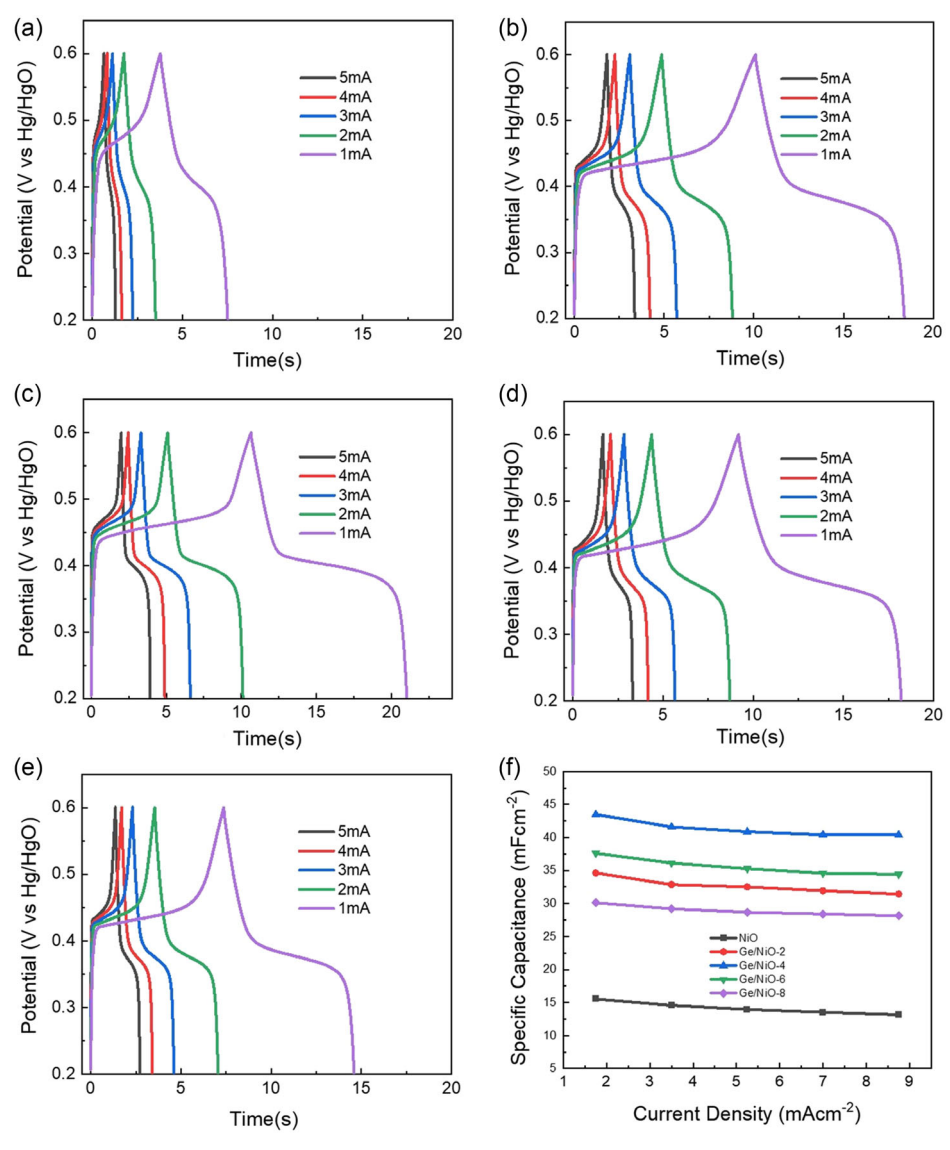


Figure 7. Galvanic charge—discharge of Ge-functionalized 3D mesoporous Ni/NiO oxides with different deposition times of Ge and after annealing 400 °C for 30 min. The data shown are a) NiO, b) GeNiO-2, c) GeNiO-4, d) GeNiO-6, e) GeNiO-8, and f) comparison of specific capacitance variation with respect to different current densities.

a three-electrode system to show the operating working potential of individual materials. Figure 9c,d shows the working of asymmetric supercapacitor in different potentials window range from 0.8 to 1.8 V. Cyclic voltammetry was measured at a scan rate of $100\,\mathrm{mVs}^{-1}$, and galvanic charge–discharge was measured at a current of 5 mA. The cyclic voltammetry response in a potential window of 0.1–1.6 V at different scan rates of 2–200 mV s⁻¹ is shown in Figure 9e. The increase in peak current with the scan rates shows the capacitive nature of asymmetric supercapacitor. The charge–discharge curve of asymmetric supercapacitor at different currents of 0.3–10 mA cm⁻² is shown in Figure 9f,g. The charge and discharge time increases with decreasing current density because electrolyte ion has more time to entre bulk into the materials at lower current density. Figure 9h shows the specific capacitance

of asymmetric supercapacitor at different scan rates. Figure 9i shows the Ragone plot of Ge-functionalized NiO and activated carbon–based asymmetric supercapacitor device. The maximum energy density of $23.8\,\mathrm{Wh\,kg^{-1}}$ (7.35 $\mu\mathrm{Wh\,cm^{-2}}$) and power density of $6.8\,\mathrm{kW\,kg^{-1}}$ (2.1 $\mathrm{mW\,cm^{-2}}$) are obtained at scan rates of 2 and $200\,\mathrm{mV\,s^{-1}}$, respectively.

The long-term stability of electrode materials was evaluated by performing a cyclic stability test, which was conducted at 5 mA cm⁻² for 10 000 cycles, as shown in **Figure 10**a. The Ge-functionalized NiO nanostructure and activated carbon–based asymmetric supercapacitor show excellent capacitance retention of 92% after 10 000 cycles. Remarkably, the Coulombic efficiency of the asymmetric supercapacitor is 97% and almost constant over 10 000 cycles. The practical applicability of asymmetric supercapacitor was demonstrated by

21944296, 2023, 10, Downloaded from https

onlinelibrary.wiley.com/doi/10.1002/ente.202300360 by The University Of Texas El Paso, Wiley Online Library on [10/07/2024]. See the Terms

nditions) on Wiley Online Library for rules of use; OA articles are governed by the applicable Creative Commons Licenso

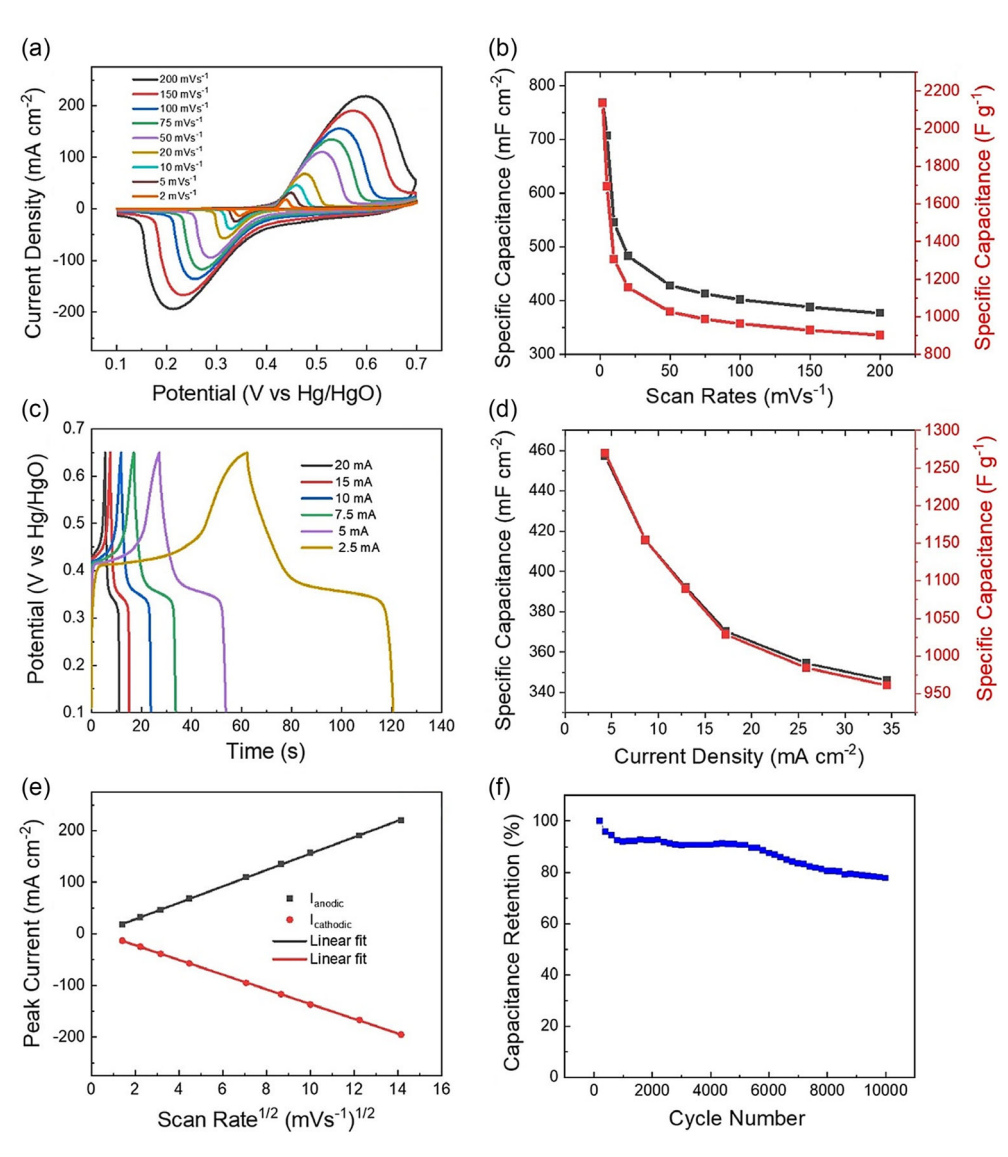


Figure 8. Electrochemical characterization data of NiO nanoflakes on Ge-functionalized 3D mesoporous Ni. The data shown are a) cyclic voltammogram at different scan rates, b) specific capacitance variation as a function of scan rates, c) galvanic charge-discharge at different currents, d) specific capacitance variation as a function of current density, e) peak current variation with scan rates, and f) cyclic stability of NiO nanoflakes at a current density of 34.5 mA cm^{-2} .

powering a digital watch for several minutes and glowing red, green, blue, yellow, and white light-emitting diode (LED), as depicted in Figure 10b,c. Some additional data on the asymmetric capacitors powering electronic devices are presented in Figure S2, Supporting Information. The digital watch was powered by a single asymmetric supercapacitor, while to glow different color LED, two asymmetric supercapacitors were connected in series. The charging current used in both cases was 0.5 mA cm^{-2} .

3. Conclusions

In the present work, we demonstrate the enhanced performance of supercapacitor by incorporating Ge at the 3D mesoporous Ni/NiO interface. In our approach, Ge-functionalized NiO enables the 3D mesoporous Ni with an interconnected framework to provide high surface area and excellent ionic conductivity. Germanium improves the electrical conductivity of NiO by reducing charge-transfer resistance. Germanium incorporation in 3D Ni and NiO interface enhances the specific capacitance of NiO significantly. The asymmetric supercapacitor shows the specific capacitance of 304 Fg⁻¹ (94 mF cm⁻²), energy density of 23.8 Wh kg⁻¹ (7.35 μ W h cm⁻²), and power density of $6.8\,\mathrm{kW\,kg^{-1}}$ ($2.1\,\mathrm{mW\,cm^{-2}}$) with excellent cyclic stability of 92% after 10 000 cycles. The asymmetric supercapacitor has enabled digital watch to run for several minutes and glow different color LED, which demonstrates the practical device application potential of the Ge-functionalized NiO electrodes in supercapacitors.

21944296, 2023, 10, Downloaded from https

/onlinelibrary.wiley.com/doi/10.1002/ente.202300360 by The University Of Texas El Paso, Wiley Online Library on [10/07/2024]. See the Terms and Conditions

and-conditions) on Wiley Online Library for rules of use; OA articles are governed by the applicable Creative Commons License

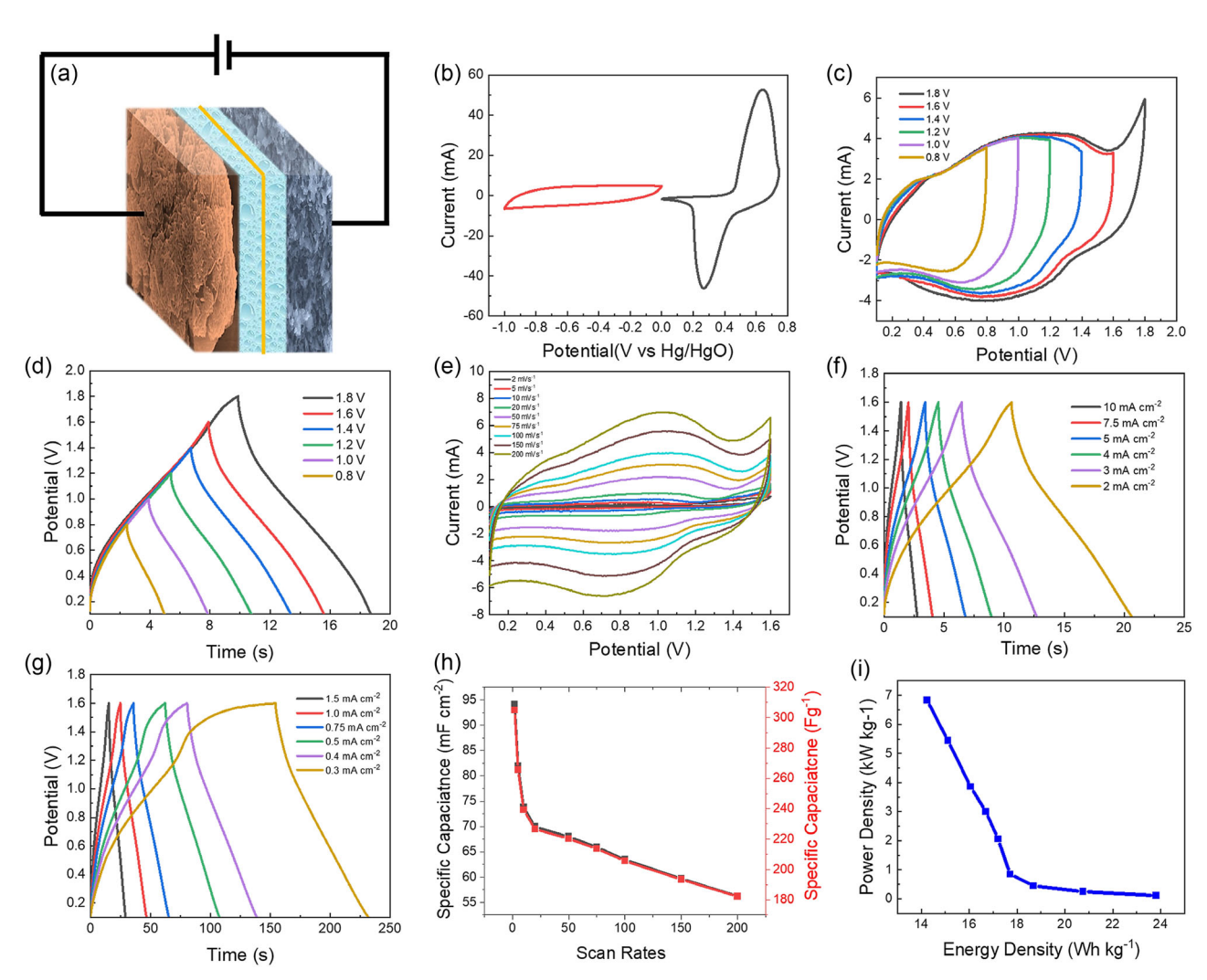


Figure 9. Electrochemical performance characteristics of asymmetric supercapacitors. a) Schematic of germanium-functionalized NiO nickel oxide nanostructure as positive and activated carbon as negative electrode, b) cyclic voltammogram of Ge-functionalized NiO and activated carbon in the three-electrode system at a scan rate of 100 mV s^{-1} , c) cyclic voltammetry of supercapacitor operating in different potential windows at a scan rate of 100 mV s⁻¹, d) galvanic charge–discharge operating in different potential windows at a current of 5 mA, e) cyclic voltammogram at different scan rates, f,g) galvanic charge-discharge at different current, h) specific capacitance at different scan rates, and i) Ragone plot at different scan rates.

4. Experimental Section

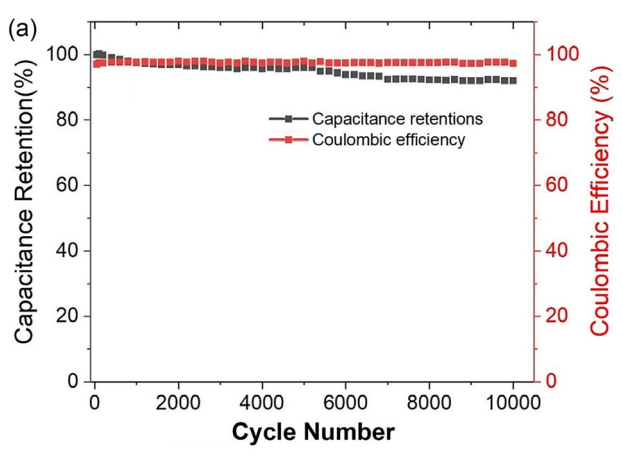
Chemicals and Reagents: All chemical reagents were of reagent grade and have been used without any further purification. Potassium hydroxide (KOH), hydrochloric acid (37%), nickel sulfate hexahydrate (NiSO₄.6H₂O), ammonium chloride (NH₄Cl), polyethylene glycol, sodium acetate, sodium sulfate (Na₂SO₄) copper (99.98%), nafion perfluorinated resin solution, ethanol, and sodium sulfate were purchased from Sigma-Aldrich. The carbon-black Super-P was perched from Alpha Aesar, and activated carbon was obtained from US Research Nanomaterials, Inc. Distilled water has been used in all experiments for making solutions and cleaning.

Materials Synthesis: Electrodeposition of Microporous Nickel: The growth of microporous Ni onto Cu substrate was carried out using a galvanostatic electrodeposition process. The electrodeposition was performed using a two-electrode setup, where nickel foam and copper substrate were used as counter and working electrodes, respectively. Prior to the deposition, Cu substrate was cleaned in 1 M HCl solution and deionized water. The bath for the synthesis of microporous nickel was prepared by adding $0.12\,\mathrm{M}$

nickel sulfate hexahydrate, 1 M ammonium chloride, and polyethylene glycol (100 mg in 300 mL) in deionized water. [45] Then, the beaker containing the aqueous bath was sonicated for 5 min to get a stable light green solution. The electrodeposition was done at current $100\,\mathrm{mA\,cm^{-2}}$ for 3 min. After the deposition, samples were cleaned in deionized water and kept at 60°C for 1 h in an oven.

The use of Ni in this work is primarily based on the following considerations. The electrical conductivity and surface area of the substrate are two important factors that affect the performance of a supercapacitor. Microporous Ni with 3D continuous network and interconnected pores is an attractive and promising material to be used as substrate. Due to its high surface area and electrical conductivity, Ni was in use as an attractive substrate for loading active electrode materials for supercapacitors with high energy and power densities. Nanoporous gold (Au) with interconnected porous network was also widely used for energy storage and conversion devices, such as batteries, supercapacitors, and electrocatalysis. $^{[32,44]}$ However, Ni was of low cost compared to Au with almost similar properties and was used in the form of films, foils, and foam for all energyrelated applications.

www.entechnol.de



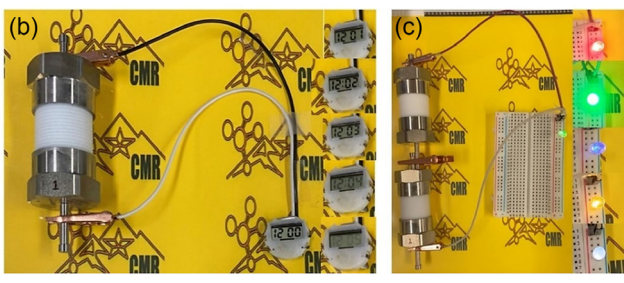


Figure 10. Cyclic stability test and practical device applicability demonstration of Ge-functionalized NiO nanostructure and activated carbon-based asymmetric supercapacitor. a) Cyclic stability and Coulombic efficiency of asymmetric supercapacitor, b) digital watch working for several minutes with the power of a single supercapacitor, and c) glowing different color light-emitting diode (LED) with two asymmetric supercapacitors connected in series.

Materials Synthesis: Surface Functionalization by Germanium: The deposition of Ge on 3D microporous Ni was done using an in-house developed sputter-deposition system. The deposition time of Ge was varied to determine the optimum quantity of Ge-surface functionalization needed to achieve enhanced electrochemical performance. The Ge-deposition time varied in the range of 0-8 min with a 2 min interval. After Ge-functionalization, all samples were annealed in controlled atmospheric condition (\approx 3 \times 10⁻² Torr) at 400 °C for 30 min. The samples were named NiO, GeNiO-2, GeNiO-4, GeNiO-6, and GeNiO-8 based on the Ge-deposition time, which was variable to produce a variable amount of Ge on the surface of Ni electrodes.

Materials Synthesis: Electrodeposition of Nickel Oxides Nanostructure: The electrodeposition of nickel oxides was done at a constant current density of 1 mA cm $^{-2}$ for 30 min. The aqueous bath was prepared by mixing 0.13 M sodium acetate, 0.13 M nickel sulfate, and 0.1 M sodium sulfate in deionized water. [46] The pH of the bath was adjusted to \approx 7 by adding

Materials Characterization: XRD patterns of mesoporous Ni and NiO oxide were recorded using a Malvern Panalytical Empyrean Nano edition multipurpose X-ray diffractometer. The X-ray diffractometer was used in Bragg-Brentano reflection geometry. All the measurements were performed at room temperature. A Cu $K\alpha$ X-ray source with a wavelength of 0.154 nm was used to acquire the measurements. A scanning electron microscope (SEM) was used to visualize the surface morphology of microporous Ni and NiO. A Hitachi-4800 field-emission FE-SEM was explored to capture the images. All the images were captured with a secondary electron detector. Energy-dispersive X-ray spectroscopy was applied to know the elemental composition, while element content mapping allowed the determination of the distribution of elements of nickel oxide.

Electrochemical Characterization and Performance Evaluation: The electrochemical deposition and characterization of all the samples were done using an Ametek Solartron Analytical (ModuLab XM) potentiostat. The electrochemical measurement was done in a three-electrode system, where platinum wire, Hg/HgO, and germanium-functionalized nickel oxides were used as counter, reference, and working electrodes, respectively. In the three-electrode system, potential was measured between the working electrode and reference electrode, whereas current was measured between the working and counter electrode. Aqueous 3M KOH was used as an electrolyte for all electrochemical measurements. The areal capacitance (C_A) , specific energy (E_A) , and specific power (P_A) of nickel

$$C_{\rm A}({\rm Fcm^{-2}}) = \frac{\int_{-V}^{V} i dV}{V(\frac{dV}{dt})A} \tag{2}$$

oxide were calculated from cyclic voltammetry by using the following

$$E_{\rm A}({\rm Wh\,cm^{-2}}) = \frac{1}{8\times3600}\,C_{\rm A}V^2 \tag{3}$$

$$P_{\rm A}\,(\,{\rm W\,cm^{-2}}) = \frac{E_{\rm A}}{V} \times \left(\frac{{\rm d}V}{{\rm d}t}\right) \times 3600 \tag{4}$$

where C_A is the areal capacitance (F cm⁻²), V is the potential window (V), $\frac{dV}{dt}$ is the scan rate (V s⁻¹), and A is the area (cm²) of the electrode. The asymmetric supercapacitor was fabricated using Ge-NiO as the positive electrode and activated carbon as the negative electrode. The area of both electrodes was 0.81 cm⁻². The mass loading of activated carbon electrode was 0.5 mg cm⁻². The mass of nickel oxides nanoflakes was adjusted to balance the charge by reducing the electrodeposition time to 8 min. The electrochemical measurements were done in 1 M KOH electrolyte. The mass and charge balance were made by following equation[47,48]

$$\frac{m^{+}}{m^{-}} = \frac{C^{-}V^{-}}{C^{+}V^{+}} \tag{5}$$

Supporting Information

equations.[42,43]

Supporting Information is available from the Wiley Online Library or from the author.

Acknowledgements

The authors acknowledge, with pleasure, the support from the National Science Foundation (NSF) with NSF-PREM grant #DMR-1827745.

Conflict of Interest

The authors declare no conflict of interest.

Data Availability Statement

The data that support the findings of this study are available from the corresponding author upon reasonable request.

Keywords

electrodeposition, germanium, nickel oxide, supercapacitors, surface functionalization, 3D mesoporous nickel

> Received: April 3, 2023 Revised: May 26, 2023

Published online: September 1, 2023

4DVANCED

21944296, 2023, 10, Downloaded from https://onlinelibrary.wiley.com/doi/10.1002/ente.202300360 by The University Of Texas El Paso, Wiley Online Library on [10.07/2024]. See the Terms and Conditions

(https://onlinelibrary.wiley.com/term

and-conditions) on Wiley Online Library for rules of use; OA articles are governed by the applicable Creative Commons License

- [1] T. Tian, H. Gao, X. Zhou, L. Zheng, J. Wu, K. Li, Y. Ding, ACS Energy Lett. 2018, 3, 2150.
- [2] N. Li, R. Guo, W. Chen, V. Körstgens, J. E. Heger, S. Liang, C. J. Brett, M. A. Hossain, J. Zheng, P. S. Deimel, A. Buyruk, F. Allegretti, M. Schwartzkopf, J. G. C. Veinot, G. Schmitz, J. V. Barth, T. Ameri, S. V. Roth, P. Müller-Buschbaum, Adv. Funct. Mater. **2021**, *31*, 2102105.
- [3] N. Attarzadeh, D. Das, S. N. Chintalapalle, S. Tan, V. Shutthanandan, C. V. Ramana, ACS Appl. Mater. Interfaces 2023, 15, 22036.
- [4] P. Simon, Y. Gogotsi, Nat. Mater. 2008, 7, 845.
- [5] B. Dunn, H. Kamath, J.-M. Tarascon, Science 2011, 334, 928.
- [6] X. Xiao, X. Li, S. Zheng, J. Shao, H. Xue, H. Pang, Adv. Mater. Interfaces 2017, 4, 1600798.
- [7] A. Lakshmi-Narayana, M. Dhananjaya, C. M. Julien, S. W. Joo, C. V. Ramana, ACS Appl. Mater. Interfaces 2023, 15, 20925.
- [8] M. Satish, H. M. Shashanka, S. Saha, K. Haritha, D. Das, P. N. Anantharamaiah, C. V. Ramana, ACS Appl. Mater. Interfaces 2023, 15, 15691.
- [9] S. Chu, A. Majumdar, Nature 2012, 488, 294.
- [10] Y. Qian, J. Zhang, J. Jin, S. Yang, G. Li, ACS Appl. Energy Mater. 2022, 5. 5830.
- [11] T. M. Dinh, A. Achour, S. Vizireanu, G. Dinescu, L. Nistor, K. Armstrong, D. Guay, D. Pech, Nano Energy 2014, 10, 288.
- [12] J. Chen, P. S. Lee, Adv. Energy Mater. 2021, 11, 2003311.
- [13] Y. Shao, M. F. El-Kady, J. Sun, Y. Li, Q. Zhang, M. Zhu, H. Wang, B. Dunn, R. B. Kaner, Chem. Rev. 2018, 118, 9233.
- [14] L. Lin, S. Piao, Y. Choi, L. Lyu, H. Hong, D. Kim, J. Lee, W. Zhang, Y. Piao, EnergyChem 2022, 4, 100072.
- [15] W. Zhang, B. Quan, C. Lee, S.-K. Park, X. Li, E. Choi, G. Diao, Y. Piao, ACS Appl. Mater. Interfaces 2015, 7, 2404.
- [16] W. Zhang, Y. Kong, X. Jin, B. Yan, G. Diao, Y. Piao, Electrochim. Acta **2020**, 331, 135345.
- [17] F. Guo, J. Guo, Z. Zheng, T. Xia, A. N. Chishti, L. Lin, W. Zhang,
- G. Diao, Chin. Chem. Lett. 2022, 33, 4846. [18] J. Wang, P. Yang, X. Wei, ACS Appl. Mater. Interfaces 2015, 7,
- 3816. [19] M. Lee, H.-S. Oh, M. K. Cho, J.-P. Ahn, Y. J. Hwang, B. K. Min, Appl.
- Catal. B 2018, 233, 130. [20] P. Kartikay, D. Sadhukhan, A. Yella, S. Mallick, Sol. Energy Mater. Sol.
- Cells 2021, 230, 111241. [21] Y.-Y. Sun, Y.-Y. Wang, G.-R. Li, S. Liu, X.-P. Gao, ACS Appl. Mater.
- Interfaces 2019, 11, 14830. [22] S. Y. Kim, T. Y. Yun, K. S. Yu, H. C. Moon, ACS Appl. Mater. Interfaces
- 2020, 12, 51978.
- [23] S. K. Meher, P. Justin, G. Ranga Rao, ACS Appl. Mater. Interfaces 2011,
- [24] V. S. Puli, R. Picchini, C. Orozco, C. V. Ramana, Chem. Phys. Lett. 2016, 649, 115.

- [25] F. Lin, D. Nordlund, T.-C. Weng, R. G. Moore, D. T. Gillaspie, A. C. Dillon, R. M. Richards, C. Engtrakul, ACS Appl. Mater. Interfaces 2013, 5, 301.
- [26] Y. Jiao, C. Qu, B. Zhao, Z. Liang, H. Chang, S. Kumar, R. Zou, M. Liu, K. S. Walton, ACS Appl. Energy Mater. 2019, 2, 5029.
- [27] R. B. Rakhi, D. Cha, W. Chen, H. N. Alshareef, J. Phys. Chem. C 2011, 115, 14392.
- [28] S. Bhattacharjee, I. M. C. M. Rietjens, M. P. Singh, T. M. Atkins, T. K. Purkait, Z. Xu, S. Regli, A. Shukaliak, R. J. Clark, B. S. Mitchell, G. M. Alink, A. T. M. Marcelis, M. J. Fink, J. G. C. Veinot, S. M. Kauzlarich, H. Zuilhof, Nanoscale 2013, 5, 4870.
- [29] J. Liang, X. Li, Z. Hou, T. Zhang, Y. Zhu, X. Yan, Y. Qian, Chem. Mater. 2015, 27, 4156.
- [30] S. Fang, L. Shen, P. Nie, G. Xu, L. Yang, H. Zheng, X. Zhang, Part. Part. Syst. Character. 2015, 32, 364.
- [31] J. M. Gonçalves, A. Kumar, M. I. da Silva, H. E. Toma, P. R. Martins, K. Araki, M. Bertotti, L. Angnes, Energy Technol. 2021, 9, 2000927.
- [32] S. H. Kim, Chem. Rec. 2021, 21, 1199.
- [33] B. K. Singh, A. Shaikh, R. O. Dusane, S. Parida, Nano-Struct. Nano-Objects 2019, 17, 239.
- [34] Z. Yang, S. Bai, H. Yue, X. Li, D. Liu, S. Lin, F. Li, D. He, Mater. Lett. **2014**, 136, 107.
- [35] X. Hu, X. Tian, Y.-W. Lin, Z. Wang, RSC Adv. 2019, 9, 31563.
- [36] B. K. Singh, D. Das, N. Attarzadeh, S. N. Chintalapalle, C. V. Ramana, Nano Select 2023, 4, 145.
- [37] M.-S. Wu, G.-W. Lin, R.-S. Yang, J. Power Sources 2014, 272, 711.
- [38] A. K. Singh, D. Sarkar, G. G. Khan, K. Mandal, J. Mater. Chem. A 2013, 1, 12759.
- [39] X. Sun, G. Wang, J.-Y. Hwang, J. Lian, J. Mater. Chem. 2011, 21, 16581. [40] S.-I. Kim, J.-S. Lee, H.-J. Ahn, H.-K. Song, J.-H. Jang, ACS Appl. Mater.
- Interfaces 2013, 5, 1596. [41] Z. Luo, L. Liu, X. Yang, X. Luo, P. Bi, Z. Fu, A. Pang, W. Li, Y. Yi, ACS
- Appl. Mater. Interfaces 2020, 12, 39098. [42] B. K. Singh, A. Shaikh, R. O. Dusane, S. Parida, J. Energy Storage 2020,
- *31*, 101631. [43] B. K. Singh, R. O. Dusane, S. Parida, Mater. Sci. Eng. B 2021, 273,
- 115436 [44] B. K. Singh, A. Shaikh, S. Badrayyana, D. Mohapatra, R. O. Dusane,
- S. Parida, RSC Adv. 2016, 6, 100467. [45] Y. Xu, A. S. Menon, P. P. R. M. L. Harks, D. C. Hermes,
- L. A. Haverkate, S. Unnikrishnan, F. M. Mulder, Energy Storage Mater. 2018, 12, 69.
- [46] D. Tench, L. F. Warren, J. Electrochem. Soc. 1983, 130, 869.
- [47] S. E. Moosavifard, M. F. El-Kady, M. S. Rahmanifar, R. B. Kaner, M. F. Mousavi, ACS Appl. Mater. Interfaces 2015, 7, 4851.
- [48] P. Yu, Z. Zhang, L. Zheng, F. Teng, L. Hu, X. Fang, Adv. Energy Mater. **2016**, *6*, 1601111.